Research Square

Preprints are preliminary reports that have not undergone peer review.
They should not be considered conclusive, used to inform clinical practice,
or referenced by the media as validated information.

Macrocyclic Polyamine–Quinazoline Conjugates Show Mutant EGFR Inhibition and DNA- Damage-Associated Activity

Hao Chang
Beijing University of Chemical Technology
Changyang Lei
Beijing University of Chemical Technology
Kai Liu
Beijing University of Chemical Technology
Cenjun Li
Beijing University of Chemical Technology
Fangke Zhi
Beijing University of Chemical Technology
Wei Liu
Peking University Third Hospital
Cheng Zhang
China-Japan Friendship Hospital
Renzhong Qiao
qiao_group@163.com
Beijing University of Chemical Technology
Chao Li
Beijing University of Chemical Technology

Research Article

Keywords: NSCLC, macrocyclic polyamine, mutant EGFR inhibition, DNA-damage-associated activity, apoptosis

Posted Date: November 6th, 2026

DOI: https://doi.org/10.21203/rs.3.rs-11373456/v1

License: This work is licensed under a Creative Commons Attribution 4.0 International License.
Read Full License

Additional Declarations: No competing interests reported.

Macrocyclic Polyamine–Quinazoline Conjugates Show Mutant EGFR Inhibition and DNA-Damage-Associated Activity

Hao Chang[1], Changyang Lei[1], Kai Liu[1], Cenjun Li[1], Fangke Zhi[1], Wei Liu[2,3], Cheng Zhang[4,*], Renzhong Qiao[1,*], Chao Li[1,3,*]

[1] State Key Laboratory of Chemical Resource Engineering, Beijing University of Chemical Technology, Beijing, 100029, P. R. China

[2] Department of Pharmacy, Peking University Third Hospital, Beijing 100191, P. R. China

[3] State Key Laboratory of Neurology and Oncology Drug Development, Simcere Pharmaceutical Group, Nanjing 210042, P. R. China

[4] Department of Pharmacy, China-Japan Friendship Hospital, Beijing 100029, P. R. China

* Corresponding authors

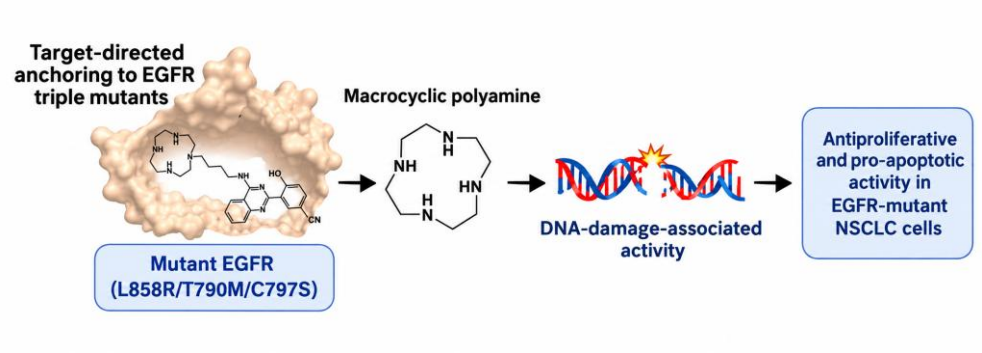
Cheng Zhang (Email: zhangcheng@zryhyy.com.cn)

Renzhong Qiao (Email: qiao_group@163.com)

Chao Li (Email: lichao@mail.buct.edu.cn)

Abstract

Resistance driven by the EGFR C797S mutation limits treatment options for non-small cell lung cancer (NSCLC). We examined macrocyclic polyamine–quinazoline conjugates for mutant EGFR inhibition and DNA-damage-associated activity. Compound 4f inhibited EGFR L858R/T790M/C797S and Del19/T790M/C797S with IC_{50} values of 0.65 and 0.85 μM, respectively, while showing weaker activity against wild-type EGFR (IC_{50} >5 μM). In 24 h cell viability assays, 4f inhibited NCI-H1975 and osimertinib-resistant H1975/OR cells, with IC_{50} values of 8.67 and 6.23 μM, respectively. PC-9 and nonmalignant BEAS-2B cells were less sensitive (IC_{50} 17.89 and 22.11 μM, respectively). Cell-free plasmid assays showed cleavage by 4f without added transition metal, whereas a matched piperazine analogue retained kinase inhibition but showed no detectable plasmid DNA cleavage. Docking and electrostatic-potential calculations suggested a possible DNA-binding mode involving the quinazoline scaffold and cationic macrocycle. In NCI-H1975 cells, comet assays showed increased DNA migration relative to vehicle-treated controls, while Annexin V-PE/7-AAD analysis detected concentration-dependent apoptosis. These findings identify 4f as a mutant EGFR inhibitor with DNA-damage-associated and pro-apoptotic cellular activities.



Keywords: NSCLC, macrocyclic polyamine, mutant EGFR inhibition, DNA-damage-associated activity, apoptosis

1. Introduction

Lung cancer causes the most cancer deaths worldwide. Non-small cell lung cancer (NSCLC) accounts for 85% of cases.[1] Abnormal activation of the epidermal growth factor receptor (EGFR) drives many NSCLC cases. Classic mutations include exon 19 deletions (Del19) and the L858R point mutation. EGFR tyrosine kinase inhibitors (TKIs) improved NSCLC treatment. Resistance mutations make first- and second-generation TKIs ineffective. [2-6] Third-generation EGFR TKIs like Osimertinib show good clinical results. Acquired resistance limits their long-term use. [7-10] The C797S mutation is the most common resistance mechanism. This mutation stops covalent bond formation. Frontline therapies fail. Researchers report many inhibitors targeting the C797S mutation. These drugs face clinical problems. The allosteric inhibitor EAI045 needs the antibody cetuximab to work. [11] It only works against the L858R/T790M/C797S variant. It fails against the Del19 variant. Brigatinib also needs an anti-EGFR antibody to kill tumors in animals. [12] Patients urgently need new single drugs to overcome C797S resistance.

Our previous work incorporated macrocyclic polyamine moieties into a 4-anilinoquinazoline scaffold and established their compatibility with EGFR inhibitor design.[13] A subsequent study explored a 2-aryl-4-aminoquinazoline series against C797S-containing EGFR mutants.[14] In that series, methyl-substituted piperazine analogues showed stronger kinase inhibition than their macrocyclic counterparts. Steric demands of the macrocycle may have limited its accommodation within the kinase pocket. Functionalized macrocyclic polyamines can also engage biological targets through their cationic amine groups.[15] We therefore examined whether retaining the macrocycle could provide DNA-associated activity alongside mutant EGFR inhibition.

We investigated macrocyclic polyamine–quinazoline conjugates for inhibition of C797S-containing EGFR mutants and DNA-damage-associated effects. Compound 4f was selected for cell-free plasmid

assays, cellular comet analysis, and apoptosis assessment. Docking suggested that EGFR binding may orient its macrocycle toward the solvent-exposed region. Increased DNA migration in treated cells was consistent with DNA strand breaks, although the comet assay cannot establish direct intracellular cleavage or its cause. The proposed design rationale is summarized in Figure 1.

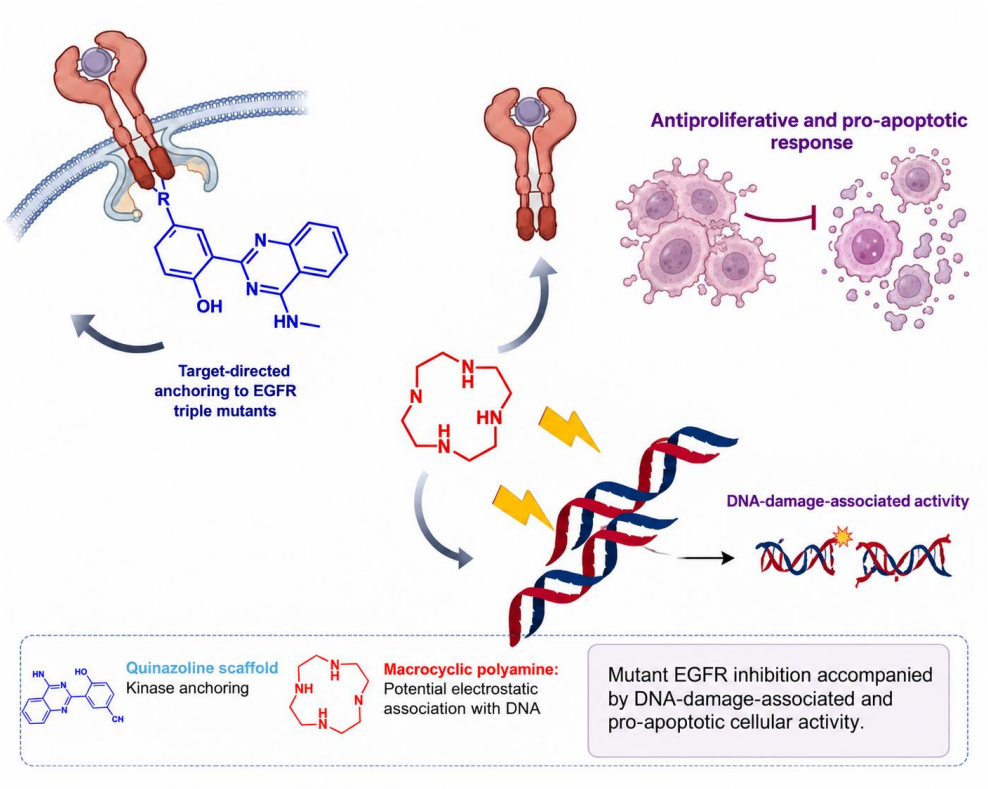


Fig. 1 Schematic representation of the proposed multifunctional activity of compound 4f. The quinazoline scaffold supports anchoring to C797S-containing mutant EGFR, whereas the cationic macrocyclic polyamine may promote DNA association, consistent with the observed DNA-damage-associated and antiproliferative/pro-apoptotic activities in EGFR-mutant NSCLC cells

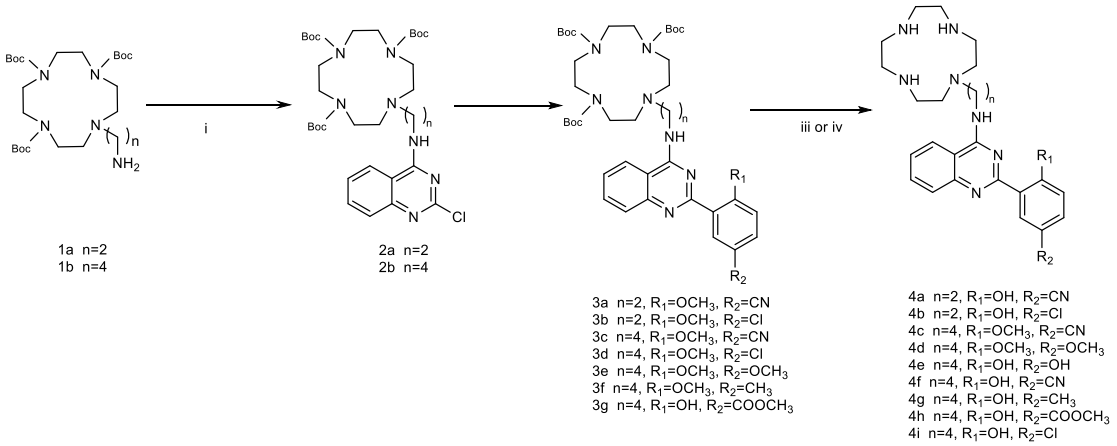
2. Results and discussion

2.1. Design and synthesis

The series was designed to vary the linker length, 2-aryl substituent, and terminal amine while retaining the quinazoline core. The macrocyclic conjugates 4a–4i were assembled by amine substitution on a 2,4-dichloroquinazoline intermediate, arylboronic acid coupling, and deprotection;

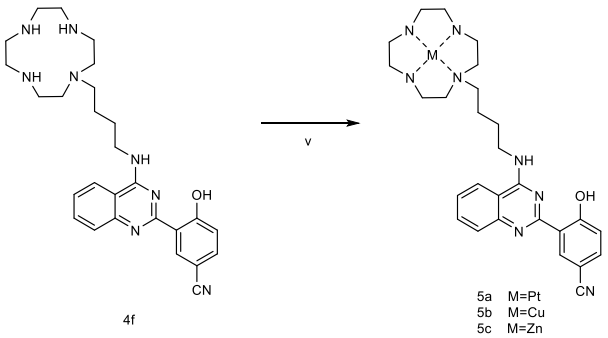
O-demethylation furnished the corresponding phenolic analogues (Scheme 1). Compound 4f was subsequently coordinated with Pt, Cu, or Zn salts (Scheme 2).

Scheme 1. Synthesis of compounds 4a–4i.



[a] Reagents and conditions: (i) THF, TEA, r.t., 18h; (ii) n-BuOH, Toluene, Na_2CO_3, $Pd(PPh_3)_4$, 90°C, 17h ; (iii)MeOH, HCl, r.t., 4h ; (iv).DCM, BBr_3, -30°C, 4h.

Scheme 2. Preparation of the 4f metal complexes (5a–5c).



a Reagents and conditions: (v) MeOH, r.t., 5 h.

2.2. Mutant EGFR inhibition and structure–activity relationships

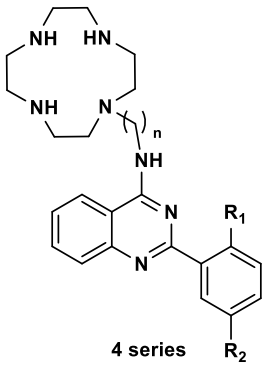
Kinase inhibition varied with the terminal amine, linker length, and substituents on the 2-phenyl ring (Table 1). With R_1 = OH and R_2 = CN, extending the linker from two carbons in 4a to four carbons in 4f improved activity against both triple mutants. The IC_{50} values decreased from >5 μM to 0.65

μM for EGFR L858R/T790M/C797S and to 0.85 μM for EGFR Del19/T790M/C797S. The chloro-substituted pair 4b and 4i showed the same trend, although the change was smaller. Activity against EGFR Del19/T790M/C797S improved from 2.10 to 0.99 μM. By contrast, piperazine derivative 6b retained strong activity with the two-carbon linker, whereas macrocyclic analogue 4a was inactive against both triple mutants. These comparisons indicate that linker length and terminal amine size are coupled. The shorter linker accommodates piperazine but appears unfavorable for the bulkier macrocycle.

Comparison of 4c and 4f showed that the free phenolic hydroxy group also favored kinase inhibition. With the four-carbon linker and cyano substituent fixed, replacing methoxy in 4c with hydroxy in 4f improved activity across all three tested variants. The gains were 3.0-fold for EGFR L858R/T790M, 3.9-fold for EGFR L858R/T790M/C797S, and at least 5.9-fold for EGFR Del19/T790M/C797S. Among hydroxy-containing analogues 4e–4i, the effect of R_2 depended on the mutation background. Compound 4f was the only macrocyclic analogue with submicromolar activity against both C797S-containing triple mutants. Compound 4e was more active against the L858R-containing triple mutant than 4h and 4i, whereas 4h and 4i were relatively more active against the Del19-containing triple mutant. The methyl analogue 4g was less active against both variants. Thus, R_2 effects did not track simply with electron-withdrawing strength and may reflect polarity, steric demand, and differences between the mutant kinase pockets. No long-linker macrocycle inhibited wild-type EGFR at concentrations up to 5 μM.

Taken together, the available compounds define a preliminary SAR. A four-carbon linker better accommodated the macrocyclic polyamine, the free phenolic hydroxy group favored mutant EGFR inhibition, and the cyano substituent gave the broadest activity across the two C797S-containing

variants. Compound 4f was therefore selected for subsequent studies because it combined the macrocyclic group with the most balanced kinase profile in the series.



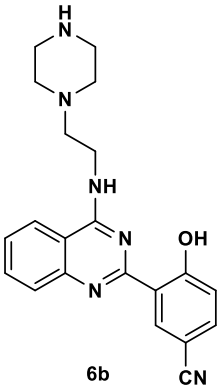


Table 1. SAR of Phenyl Ring Substituents and EGFR Kinase Selectivity.[a]

Compounds	n	R_1	R_2	EGFR IC_{50}（μM）			
				WT	L858R/T790M	L858R/T790M/C797S	Del19/T790M/C797S
4a	2	-OH	-CN	-[b]	-	>5	>5
4b	2	-OH	-Cl	-	-	>5	2.10
4c	4	$-OCH_3$	-CN	>5	4.13	2.54	>5
4d	4	$-OCH_3$	$-OCH_3$	>5	>5	>5	-
4e	4	-OH	-OH	>5	2.06	1.02	1.91
4f	4	-OH	-CN	>5	1.38	0.65	0.85
4g	4	-OH	$-CH_3$	>5	3.06	2.15	> 5
4h	4	-OH	$-COOCH_3$	>5	-	>5	1.27
4i	4	-OH	-Cl	>5	-	3.72	0.99
6b	2	-OH	-CN	-	-	0.74	0.22

[a] Enzymatic inhibitory activities (IC_{50}) were determined, following the LanthaScreen® assay protocol recommended by Invitrogen, The data represent the mean values of two independent experiments.

[b] Not determined; C797S triple-mutant profiling was prioritized, and 4d was not further tested because its other IC_{50} values were >5 μM.

2.3. Molecular docking in mutant EGFR

Compound 4f was selected for subsequent studies because it combined the most balanced triple-mutant kinase profile with the macrocyclic polyamine. Docking supported the structural rationale for this choice (Figure 2). The four-carbon linker preserved the key kinase-pocket interactions of the quinazoline core while directing the macrocycle toward the solvent-exposed region. The short-linker analogue 4a did not adopt this arrangement. We next examined the antiproliferative and DNA-damage-associated activities of 4f.

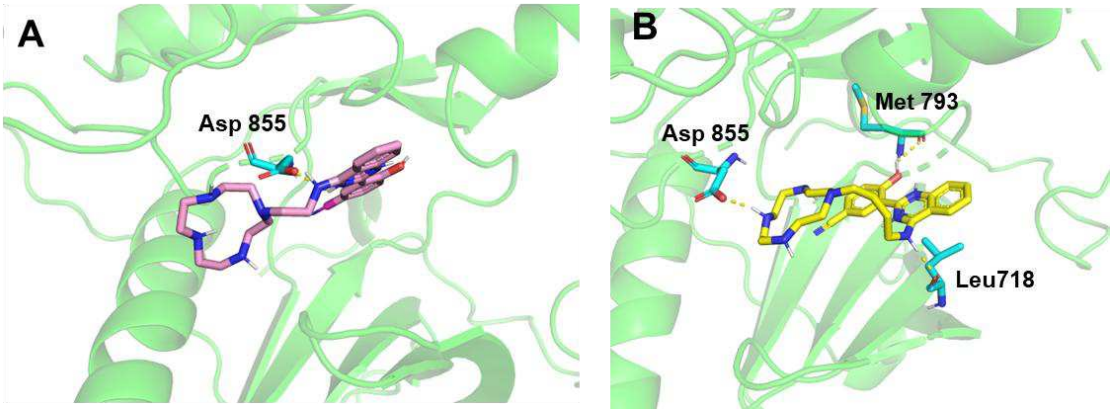


Fig. 2 Molecular docking simulations of representative compounds in the EGFR L858R/T790M/C797S kinase pocket (PDB: 6LUD). (A) Binding modes of short-linker compound 4a (pink). (B) Binding mode of the optimized butyl-linked compound 4f (cyan) highlighting critical interactions. Hydrogen bonds are depicted as yellow dashed lines

2.4. Effect of metal coordination on EGFR inhibition

To examine how metal coordination affected the kinase activity of 4f, Pt, Cu, and Zn complexes were prepared and tested (Table 2). All three complexes were less active than metal-free 4f. Compound 4f-Cu gave IC_{50} values >5 μM against both triple mutants. Compound 4f-Zn gave IC_{50} values of 2.64 and 2.77 μM. Compound 4f-Pt retained moderate activity against EGFR L858R/T790M/C797S (1.12

μM) but gave an IC_{50} value >5 μM against EGFR Del19/T790M/C797S. Metal coordination may restrict macrocycle flexibility or add steric bulk near the kinase pocket. Either effect could weaken productive positioning of the quinazoline scaffold. These results led us to evaluate the metal-free conjugate in the subsequent cellular and DNA assays.

Table 2. Kinase Inhibitory Activities of Metal-Coordinated Complexes.[a]

Compounds	EGFR IC_{50}（μM）	
	L858R/T790M/C797S	Del19/T790M/C797S
4f-Pt	1.12	>5
4f-Cu	>5	>5
4f-Zn	2.64	2.77

[a] The data represent the mean values of two independent experiments

2.5. Antiproliferative activity in NSCLC cells

Cellular growth inhibition by 4f was measured after 24 h in NCI-H1975, H1975/OR, PC-9, and nonmalignant BEAS-2B cells (Figure 3). The IC_{50} values were 8.67 μM in H1975 cells and 6.23 μM in H1975/OR cells. The similar responses show that 4f retained activity in the osimertinib-resistant model. PC-9 cells were less sensitive, with an IC_{50} value of 17.89 μM, indicating variation among EGFR-mutant backgrounds. The IC_{50} value in BEAS-2B cells was 22.11 μM, which was 2.6-fold and 3.5-fold higher than those in H1975 and H1975/OR cells, respectively. Thus, 4f showed a modest selectivity window for the two H1975-derived cancer cell models.

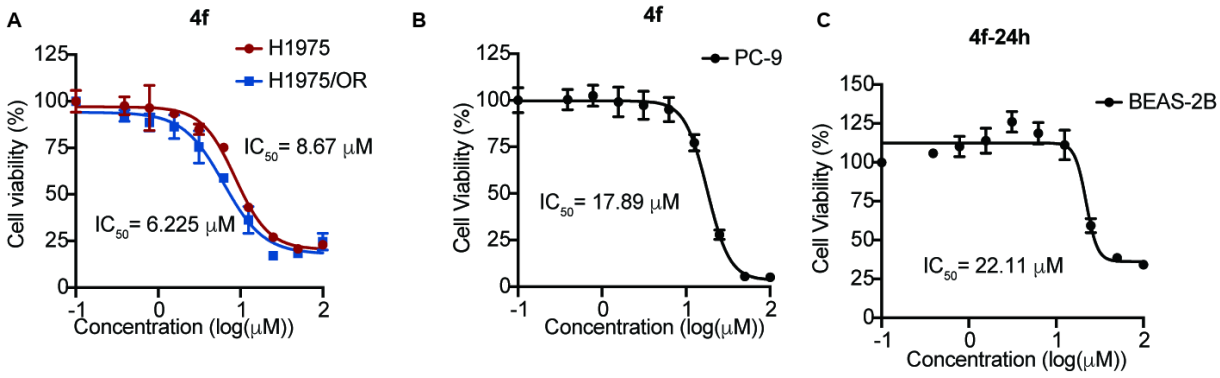


Fig. 3 Antiproliferative activity of 4f in EGFR-mutant NSCLC and nonmalignant bronchial epithelial cells. Dose–response curves after 24 h treatment are shown for (A) NCI-H1975 and H1975/OR cells, (B) PC-9 cells, and (C) BEAS-2B cells. Cell viability was measured using the CCK-8 assay and normalized to the vehicle control. Data are mean ± SD from two independent experiments

2.6. Plasmid DNA cleavage and cellular DNA damage

Cell-free plasmid cleavage was examined using supercoiled pUC18 DNA. Compound 4f produced detectable conversion from supercoiled Form I to open-circular Form II at 70 μg/mL (Figure 4A). Under the same concentration, piperazine analogue 6b produced no detectable cleavage, and Form I remained intact (Figure 4C).

Metal coordination altered plasmid cleavage in the cell-free assay. Compound 4f-Pt produced detectable cleavage at 20 μg/mL (Figure 4B). At the common test concentration, 4f-Pt caused extensive plasmid degradation, whereas 4f and 4f-Cu produced moderate cleavage (Figure 4D). These electrophoretic results establish plasmid cleavage under the assay conditions but do not establish the same process in cells.

An alkaline comet assay was then used to examine treatment-associated DNA damage in NCI-H1975 cells. Vehicle-treated cells showed compact nucleoids with little DNA migration (Figure 4E). Treatment with 4f (40 μM) or 4f-Pt (154 μM) increased comet-tail formation (Figure 4F,G), consistent with strand breaks or alkali-labile sites. The assay does not identify the origin of this migration.

Replication stress, reactive oxygen species, and apoptosis-associated fragmentation therefore remain possible contributors. The cellular observations are accordingly described as DNA-damage-associated effects rather than direct intracellular nuclease activity. ImageJ analysis of the comet images is reported in Figure S1. Across four 10× fields per condition, mean Tail DNA was 17.46 ± 3.93% for the untreated control. Values were 73.66 ± 9.92% for 4f and 45.44 ± 10.80% for 4f-Pt. Mean Olive tail moments were 5.26 ± 1.32, 48.55 ± 3.03, and 28.18 ± 11.33 pixels, respectively.

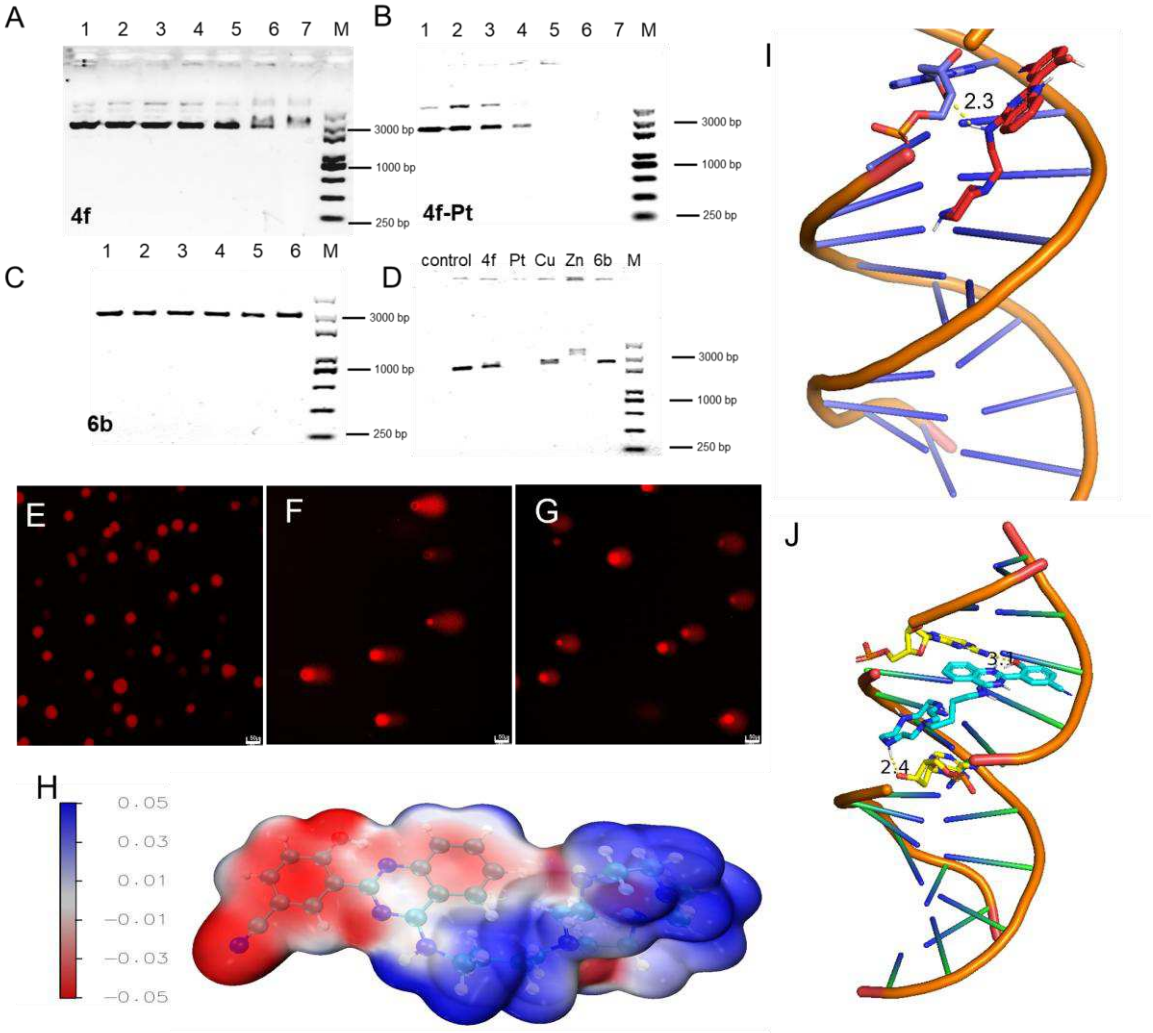


Fig. 4 Cell-free plasmid DNA cleavage, comet assays, and computational analysis of DNA association. (A,B) Agarose gel electrophoresis of supercoiled pUC18 DNA treated with 4f or 4f-Pt at 0, 5, 10, 20, 40, 70, and 110 μg/mL. (C) Plasmid DNA treated with 6b at 0, 5, 10, 20, 40, and 70 μg/mL. (D) Comparative assay at a single concentration. Lanes: untreated DNA, 4f, 4f-Pt, 4f-Cu, 4f-Zn, 6b, and DNA marker (M). (E–G) Representative comet images of NCI-H1975 cells treated with vehicle, 4f (40 μM), or 4f-Pt (154 μM). (H) Electrostatic-potential surface of 4f. (I,J) Docking poses of 6b and 4f with double-stranded DNA (PDB 1BNA)

2.7. Computational analysis of DNA association

Electrostatic-potential calculations provided a physicochemical rationale for DNA association. The quinazoline region was predominantly neutral to negative, whereas the macrocyclic polyamine

carried concentrated positive potential under the modeled conditions (Figure 4H). This distribution could favor electrostatic association of the macrocycle with the negatively charged DNA phosphate backbone.

Docking was used to examine possible interactions of 6b and 4f with double-stranded DNA. In the 6b model, the secondary amine was positioned 2.3 Å from a deoxyguanosine residue, consistent with a possible hydrogen bond (Figure 4I). This pose is compatible with DNA association but does not establish DNA damage. In the 4f model, the planar quinazoline scaffold was positioned between adjacent base pairs, while the cationic macrocycle occupied the DNA groove (Figure 4J). Macrocyclic amines were located 2.4 and 3.1 Å from phosphate oxygen atoms, consistent with possible hydrogen-bonding and electrostatic interactions. The model offers a plausible basis for DNA association.

2.8. Apoptosis in NCI-H1975 cells

Apoptosis in NCI-H1975 cells was assessed by Annexin V-PE/7-AAD flow cytometry. Treatment with 4f at 12.5, 25, and 50 μM increased the Annexin V-positive population in a concentration-dependent manner (Figure 5). Early apoptosis predominated at 12.5 and 25 μM. At 50 μM, both early and late apoptotic populations increased markedly. These data show that the cellular response to 4f was accompanied by apoptosis.

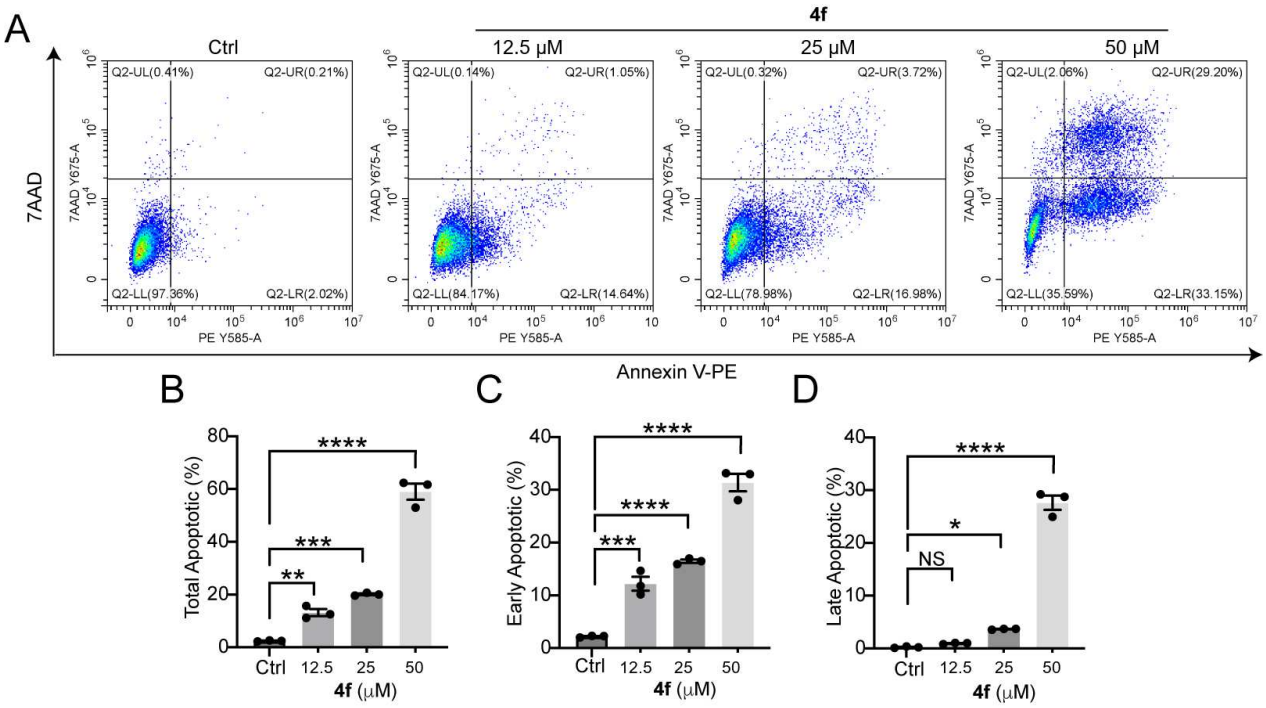


Fig. 5 Apoptosis in NCI-H1975 cells after treatment with 4f. (A) Representative Annexin V-PE/7-AAD flow-cytometry plots for vehicle-treated cells and cells exposed to 12.5, 25, or 50 μM 4f. (B–D) Total, early, and late apoptotic fractions, respectively. Statistical comparisons are shown in the panels; NS, not significant; *P < 0.05, **P < 0.01, ***P < 0.001, ****P < 0.0001

3. Conclusions

Compound 4f combined preferential inhibition of C797S-containing EGFR mutants with antiproliferative activity in EGFR-mutant NSCLC cells, including the osimertinib-resistant H1975/OR model. It cleaved plasmid DNA under cell-free conditions, increased comet-assay DNA migration, and induced apoptosis in NCI-H1975 cells. The contrast with piperazine analogue 6b, together with docking and electrostatic-potential analyses, supports a functional role for the cationic macrocycle in DNA association and plasmid cleavage. These results support further investigation of macrocyclic polyamine–quinazoline conjugates as mutant EGFR inhibitors with DNA-damage-associated cellular activity.

4. Experimental

4.1. Chemistry and compound characterization

All chemicals and solvents were obtained from commercial sources and used without further purification. Reaction progress was monitored by thin-layer chromatography (TLC) under UV light at 254 or 365 nm. Target compounds were purified via column chromatography. ^{1}H NMR and ^{13}C NMR spectra were recorded on a Bruker 400 MHz spectrometer. High-resolution mass spectrometry (HRMS) data were acquired using an Agilent QTOF 6540 instrument. Compound purity (≥95%) was determined by Waters HPLC with an Agilent C18 column (4.6 mm × 250 mm, 5 μm), employing a mobile phase consisting of (A) 0.1% formic acid in KH_2PO_4 buffer (pH 2.8), (B) methanol, and (C) acetonitrile at a flow rate of 1 mL/min. All active compounds were analyzed using PAINS filters and no PAINS substructures were identified.

4.1.1. General synthetic procedures

General Procedure 1

2,4-Dichloroquinazoline (1.0 equiv) and the corresponding aliphatic amine (1.0 equiv) were dissolved in tetrahydrofuran (0.5 M). Triethylamine (3.0 equiv) was added to the mixture. The reaction mixture was stirred at room temperature for 18 h. After completion, the solvent was removed under reduced pressure. The crude product was purified by flash chromatography using dichloromethane/methanol and/or n-hexane/ethyl acetate as the eluent system.

General Procedure 2

The chloro-substituted quinazoline or purine core (1.0 equiv), the corresponding arylboronic acid (1.1 equiv), and $Pd(PPh_3)_4$(0.01 equiv) were placed under an inert atmosphere of nitrogen. The mixture was dissolved in a solvent system consisting of n-butanol, 2 M aqueous sodium carbonate solution,

and toluene (1:1:0.5 v/v/v)(1.5 M). The reaction mixture was stirred at 90 °C for 17 h. After cooling, the mixture was filtered to remove solid residues(primarily the spent palladium catalyst). The filtrate was concentrated under reduced pressure to remove the solvents. The resulting crude product was purified by flash chromatography using dichloromethane/methanol and/or n-hexane/ethyl acetate as the eluent system.

General Procedure 3

The Boc-protected amino compound (1.0 equiv) was dissolved in methanol (0.04 M). Concentrated hydrochloric acid (12 M, 5.0 equiv) was added to the solution. The reaction mixture was stirred at room temperature for 4 h. Upon completion of the reaction, the mixture was filtered. The solid residue (the deprotected amine hydrochloride salt) was collected and dissolved in water. The aqueous solution was basified to pH 9. The free base was then extracted three times with dichloromethane/methanol (10:1, v/v). The combined organic extracts were dried over anhydrous sodium sulfate, filtered, and concentrated under reduced pressure to afford the deprotected amine product.

General Procedure 4

The methoxy-containing compound (1.0 equiv)was placed under an inert nitrogen atmosphere and dissolved in DCM (0.05 M). The solution was cooled to -30 °C (using a dry ice/isopropanol or acetone bath). BBr_3(12 equiv)was added dropwise via syringe or cannula over while maintaining the internal temperature below -25 °C. After complete addition, the reaction mixture was stirred at -30 °C for 4 h.

The reaction was quenched by the cautious dropwise addition of methanol (at -30 °C or upon warming to ~0 °C) until gas evolution subsided. The mixture was then warmed to room temperature and concentrated under reduced pressure. The crude product was purified by flash chromatography.

General Procedure 5

The macrocyclic ligand (1.0 equiv) was dissolved in methanol (0.0026 M) in a 50 mL round-bottom flask. The corresponding transition metal salt (1.0 equiv; e.g., potassium tetrachloroplatinate for compound 5a) was added to the solution. The reaction mixture was stirred at 25 °C for 5 h. Upon completion of the reaction, the resulting precipitate was collected by filtration. The collected solid was washed with a small amount of cold methanol and dried under vacuum to afford the corresponding metal complex product.

4.1.2. Synthesis and characterization of compounds

tri-tert-butyl 10-(2-((2-chloroquinazolin-4-yl)amino)ethyl)-1,4,7,10-tetraazacyclododecane-1,4,7-tricarboxylate (2a)

Following General Procedure 1 using reactant **1a** and **2,4-dichloroquinazoline**, the title compound was obtained as a yellow oily product (75.1% yield).^{1}H NMR (400 MHz, DMSO-d_6) δ 3.42 (s, 2H), 3.25 (s, 4H), 2.66 (t, J = 7.2 Hz, 2H), 2.56 (dd, J = 14.2, 8.5 Hz, 4H), 1.44 – 1.37 (m, 27H).

tri-tert-butyl 10-(4-((2-chloroquinazolin-4-yl)amino)butyl)-1,4,7,10-tetraazacyclododecane-1,4,7-tricarboxylate (2b)

Following General Procedure 1 using reactant **1b** and **2,4-dichloroquinazoline**, the title compound was obtained as a yellow oily product (70.0% yield).^{1}H NMR (400 MHz, Chloroform-*d*) δ 2.83 (d, J = 6.5 Hz, 2H), 3.54 (d, J = 18.5 Hz, 5H), 3.37 – 3.23 (m, 9H), 2.75 – 2.48 (m, 6H), 1.53 (p, J = 3.6 Hz, 4H), 1.47 (d, J = 7.8 Hz, 27H).

tri-tert-butyl 10-(2-((2-(5-cyano-2-methoxyphenyl)quinazolin-4-yl)amino)ethyl)-1,4,7,10-tetraazacyclododecane-1,4,7-tricarboxylate (3a)

Following General Procedure 2 using reactant **2a** and (5-cyano-2-methoxyphenyl)boronic acid, the title compound was obtained as a white oily product (56.0% yield).^{1}H NMR (400 MHz, Chloroform-*d*) δ 8.06 (d, *J* = 2.2 Hz, 2H), 7.94 (d, *J* = 8.3 Hz, 1H), 7.76 (ddd, *J* = 8.4, 7.0, 1.3 Hz, 1H), 7.71 (dd, *J* = 8.6, 2.2 Hz, 1H), 7.48 (ddd, *J* = 8.2, 6.9, 1.2 Hz, 1H), 7.08 (d, *J* = 8.7 Hz, 1H), 3.93 (s, 3H), 3.84 (d, *J* = 5.8 Hz, 2H), 3.56 (s, 4H), 3.38 (s, 8H), 2.92 (t, *J* = 6.3 Hz, 2H), 2.76 (s, 4H), 1.48 (s, 27H).

tri-tert-butyl 10-(2-((2-(5-chloro-2-methoxyphenyl)quinazolin-4-yl)amino)ethyl)-1,4,7,10-tetraazacyclododecane-1,4,7-tricarboxylate (3b)

Following General Procedure 2 using reactant **2a** and (5-chloro-2-methoxyphenyl)boronic acid, the title compound was obtained as a yellow oily product (65.0% yield).^{1}H NMR (400 MHz, Chloroform-*d*) δ 8.00 – 7.89 (m, 2H), 7.78 – 7.69 (m, 2H), 7.46 (ddd, *J* = 8.2, 6.9, 1.2 Hz, 1H), 7.34 (dd, *J* = 8.8, 2.7 Hz, 1H), 6.95 (d, *J* = 8.8 Hz, 1H), 3.85 (s, 5H), 3.44 (d, *J* = 75.7 Hz, 12H), 2.93 (t, *J* = 6.7 Hz, 2H), 2.76 (d, *J* = 5.9 Hz, 4H), 1.48 (s, 27H).

tri-tert-butyl 10-(4-((2-(5-cyano-2-methoxyphenyl)quinazolin-4-yl)amino)butyl)-1,4,7,10-tetraazacyclododecane-1,4,7-tricarboxylate (3c)

Following General Procedure 2 using reactant **2b** and (5-cyano-2-methoxyphenyl)boronic acid, the title compound was obtained as a yellow oily product (68.0% yield).^{1}H NMR (400 MHz, Chloroform-*d*) δ 8.24 – 7.96 (m, 3H), 7.80 – 7.70 (m, 2H), 7.49 (t, *J* = 7.7 Hz, 1H), 7.11 (d, *J* = 8.7 Hz, 1H), 3.98 (s, 3H), 3.77 (s, 2H), 3.68 – 3.27 (m, 12H), 2.71 (s, 4H), 1.83 (t, *J* = 4.0 Hz, 2H), 1.72 – 1.56 (m, 4H), 1.56 – 1.44 (m, 27H).

tri-tert-butyl 10-(4-((2-(5-chloro-2-methoxyphenyl)quinazolin-4-yl)amino)butyl)-1,4,7,10-tetraazacyclododecane-1,4,7-tricarboxylate (3d)

Following General Procedure 2 using reactant **2b** and (5-chloro-2-methoxyphenyl)boronic acid, the title compound was obtained as a yellow-green oily product (67.0% yield).^{1}H NMR (400 MHz, Chloroform-*d*) δ 7.92 (dd, *J* = 8.3, 1.2 Hz, 1H), 7.79 (d, *J* = 2.7 Hz, 1H), 7.76 – 7.67 (m, 1H), 7.52 – 7.41 (m, 2H), 7.35 (dd, *J* = 8.8, 2.7 Hz, 1H), 6.97 (d, *J* = 8.9 Hz, 1H), 3.88 (s, 3H), 3.74 (q, *J* = 6.4 Hz, 2H), 3.64 – 3.19 (m, 14H), 2.68 (s, 6H), 1.81 (p, *J* = 6.8, 6.3 Hz, 2H), 1.48 (d, *J* = 7.9 Hz, 27H).

tri-tert-butyl 10-(4-((2-(2,5-dimethoxyphenyl)quinazolin-4-yl)amino)butyl)-1,4,7,10-tetraazacyclododecane-1,4,7-tricarboxylate (3e)

Following General Procedure 2 using reactant **2b** and (2,5-dimethoxyphenyl)boronic acid, the title compound was obtained as a white oily product (65.0% yield).^{1}H NMR (400 MHz, DMSO-d_6) δ 8.36 – 8.19 (m, 2H), 7.76 (ddd, *J* = 8.1, 6.8, 1.2 Hz, 1H), 7.70 (dd, *J* = 8.4, 1.3 Hz, 1H), 7.50 (ddd, *J* = 8.2, 6.8, 1.4 Hz, 1H), 7.14 (d, *J* = 3.2 Hz, 1H), 7.05 (d, *J* = 8.9 Hz, 1H), 6.97 (dd, *J* = 8.9, 3.2 Hz, 1H), 3.74 (d, *J* = 5.8 Hz, 6H), 3.59 (q, *J* = 6.9 Hz, 4H), 3.17 (s, 14H), 1.66 (t, *J* = 7.2 Hz, 2H), 1.50 (s, 2H), 1.42 – 1.36 (m, 27H).

tri-tert-butyl 10-(4-((2-(2-methoxy-5-methylphenyl)quinazolin-4-yl)amino)butyl)-1,4,7,10-tetraazacyclododecane-1,4,7-tricarboxylate (3f)

Following General Procedure 2 using reactant **2b** and (2-methoxy-5-methylphenyl)boronic acid, the title compound was obtained as a white oily product (50.0% yield).^{1}H NMR (400 MHz, Chloroform-*d*) δ 8.05 (d, *J* = 8.3 Hz, 1H), 7.91 (dd, *J* = 8.4, 1.2 Hz, 1H), 7.70 (ddd, *J* = 8.3, 7.0, 1.3 Hz, 1H), 7.62 (d, *J* = 2.3 Hz, 1H), 7.47 – 7.38 (m, 1H), 7.21 (dd, *J* = 8.4, 2.3 Hz, 1H), 6.94 (d, *J* = 8.4 Hz, 1H), 3.87 (s, 3H), 3.75 (t, *J* = 6.7 Hz, 2H), 3.64 – 3.26 (m, 14H), 2.66 (t, *J* = 8.3 Hz, 4H), 1.81 (p, *J* = 6.9 Hz, 2H), 1.60 (q, *J* = 8.2, 7.4 Hz, 2H), 1.49 (s, 27H).

tri-tert-butyl 10-(4-((2-(2-hydroxy-5-(methoxycarbonyl)phenyl)quinazolin-4-yl)amino)butyl)-1,4,7,10-tetraazacyclododecane-1,4,7-tricarboxylate (3g)

Following General Procedure 2 using reactant **2b** and (2-hydroxy-5-(methoxycarbonyl)phenyl)boronic acid, the title compound was obtained as a yellow-white oily product (80.0% yield).^{1}H NMR (400 MHz, Chloroform-*d*) δ 9.25 (dd, *J* = 15.1, 2.3 Hz, 1H), 8.04 (ddd, *J* = 8.0, 5.7, 2.3 Hz, 1H), 7.81 (d, *J* = 8.3 Hz, 1H), 7.79 – 7.65 (m, 2H), 7.54 – 7.40 (m, 2H), 7.04 (dd, *J* = 8.5, 3.4 Hz, 1H), 3.94 (s, 3H), 3.91 – 3.22 (m, 16H), 2.71 (s, 4H), 2.15 – 1.70 (m, 4H), 1.49 (d, *J* = 6.1 Hz, 27H).

3-(4-((2-(1,4,7,10-tetraazacyclododecan-1-yl)ethyl)amino)quinazolin-2-yl)-4-hydroxybenzonitrile (4a)

Following General Procedure 4 using reactant **3a**, the title compound was obtained as a white solid product (17.0% yield). ^{1}H NMR (400 MHz, Methanol-d_4) δ 8.20 – 8.06 (m, 2H), 7.79 – 7.69 (m, 2H), 7.53 – 7.39 (m, 2H), 6.80 (d, *J* = 8.7 Hz, 1H), 3.84 (t, *J* = 6.8 Hz, 2H), 2.92 (t, *J* = 6.8 Hz, 3H), 2.82 – 2.60 (m, 14H), 2.56 (d, *J* = 5.2 Hz, 4H). HRMS(ESI) m/z: ($[M+H]^+$) calcd. For $C_{25}H_{33}N_8O^+$：461.2772，Found: 461.2418. HPLC:99.90%

2-(4-((2-(1,4,7,10-tetraazacyclododecan-1-yl)ethyl)amino)quinazolin-2-yl)-4-chlorophenol (4b)

Following General Procedure 4 using reactant **3b**, the title compound was obtained as a white solid product (19.0% yield). ^{1}H NMR (400 MHz, Methanol-d_4) δ 8.39 (d, *J* = 2.7 Hz, 1H), 8.01 (dd, *J* = 8.3, 1.3 Hz, 1H), 7.73 (ddt, *J* = 10.5, 4.9, 2.5 Hz, 1H), 7.67 – 7.63 (m, 1H), 7.45 (ddd, *J* = 8.2, 6.8, 1.4 Hz, 1H), 7.32 – 7.20 (m, 1H), 6.88 (dd, *J* = 8.7, 2.8 Hz, 1H), 3.77 (dd, *J* = 7.9, 6.1 Hz, 2H), 2.90 (dd, *J* = 7.9, 6.1 Hz, 2H), 2.69 (dddd, *J* = 24.2, 15.4, 12.9, 5.3 Hz, 14H), 2.51 (dd, *J* = 6.7, 3.7 Hz, 4H). ^{13}C NMR (101 MHz, CD_3OD_SPE) δ 160.19, 159.73, 159.42, 146.90, 133.02, 131.46, 128.21, 126.04, 125.82, 122.59, 122.03, 120.67, 118.59, 113.69, 51.84, 50.80, 45.77, 45.00, 44.01, 38.45.

HRMS(ESI) m/z: ([M+H]$^+$) calcd. For $C_{24}H_{33}ClN_7O^+$：470.2430，Found: 470.2378.

HPLC:96.02%

3-(4-((4-(1,4,7,10-tetraazacyclododecan-1-yl)butyl)amino)quinazolin-2-yl)-4-methoxybenzonitrile (4c)

Following General Procedure 3 using reactant **3c**, the title compound was obtained as a white solid product (79.0% yield). ^{1}H NMR (400 MHz, DMSO-d_6) δ 8.32 – 8.24 (m, 1H), 7.97 – 7.93 (m, 1H), 7.90 (dd, J = 8.6, 2.3 Hz, 1H), 7.81 – 7.73 (m, 1H), 7.70 (d, J = 8.3 Hz, 1H), 7.57 – 7.47 (m, 1H), 3.89 – 3.79 (m, 3H), 3.54 (d, J = 6.3 Hz, 2H), 2.60 – 2.52 (m, 6H), 2.50 – 2.36 (m, 12H), 1.76 – 1.63 (m, 2H), 1.48 (dd, J = 14.5, 7.1 Hz, 2H). ^{13}C NMR (101 MHz, DMSO-d_6) δ 161.20, 160.22, 159.97, 150.00, 134.66, 133.00, 131.98, 129.29, 127.96, 126.01, 123.56, 119.52, 114.05, 113.69, 102.75, 65.03, 56.65, 54.77, 50.69, 47.43, 45.99, 44.75, 30.46, 26.62, 23.93, 19.11, 14.01.HRMS(ESI) m/z: ([M+H]$^+$) calcd. For $C_{28}H_{39}N_8O^+$：503.3242，Found: 503.3246.

HPLC:97.55%

***N*-(4-(1,4,7,10-tetraazacyclododecan-1-yl)butyl)-2-(2,5-dimethoxyphenyl)quinazolin-4-amine (4d)**

Following General Procedure 3 using reactant **3e**, the title compound was obtained as a white solid product (75.0% yield). ^{1}H NMR (400 MHz, Methanol-d_4) δ 8.51 (d, J = 8.2 Hz, 1H), 8.05 (t, J = 7.7 Hz, 1H), 7.97 (d, J = 8.3 Hz, 1H), 7.88 (d, J = 2.6 Hz, 1H), 7.79 (t, J = 7.7 Hz, 1H), 7.35 – 7.30 (m, 2H), 4.09 (s, 3H), 4.01 (t, J = 6.1 Hz, 2H), 3.91 (s, 3H), 3.38 (d, J = 12.8 Hz, 18H), 2.04 (s, 2H), 1.99 – 1.92 (m, 2H). ^{13}C NMR (101 MHz, DMSO-D_6) δ 160.16, 159.14, 153.42, 152.20, 134.65, 132.63, 132.06, 129.37, 127.22, 124.65, 123.80, 117.60, 116.72, 114.61, 113.21, 57.30, 56.19, 52.38, 48.38, 44.95, 42.85, 42.60, 28.59, 26.68, 21.82. HRMS(ESI) m/z: ([M+H]$^+$) calcd. For $C_{28}H_{42}N_7O_2^+$：508.3395，Found: 508.3402. HPLC:95.13%

2-(4-((4-(1,4,7,10-tetraazacyclododecan-1-yl)butyl)amino)quinazolin-2-yl)benzene-1,4-diol (4e)

Following General Procedure 4 using reactant **3e**, the title compound was obtained as a yellow solid product (20.0% yield).^{1}H NMR (400 MHz, Methanol-d_4) δ 8.57 (s, 2H), 8.11 (d, J = 8.2 Hz, 1H), 8.00 (d, J = 3.0 Hz, 1H), 7.77 (dd, J = 7.7, 6.3 Hz, 1H), 7.71 (dd, J = 8.4, 1.4 Hz, 1H), 7.48 (ddd, J = 8.2, 6.7, 1.3 Hz, 1H), 6.85 (dd, J = 3.4, 1.7 Hz, 1H), 6.80 (d, J = 8.7 Hz, 1H), 3.81 (t, J = 6.2 Hz, 2H), 3.00 – 2.26 (m, 18H), 1.69 – 1.66 (m, 2H), 1.31 (s, 2H). ^{13}C NMR (101 MHz, DMSO-D_6) δ 161.31, 159.50, 154.20, 149.44, 147.57, 133.98, 132.07, 131.97, 129.28, 126.66, 126.16, 124.09, 120.84, 119.75, 118.11, 114.80, 113.98, 52.67, 49.09, 48.51, 45.22, 43.12, 42.73, 41.23, 26.87, 21.87. HRMS(ESI) m/z: ([M+H] $^{+}$) calcd. For $C_{26}H_{38}N_7O_2^{+}$: 480.3082, Found: 480.3079. HPLC:97.42%

3-(4-((4-(1,4,7,10-tetraazacyclododecan-1-yl)butyl)amino)quinazolin-2-yl)-4-hydroxybenzonitrile (4f)

Following General Procedure 4 using reactant **3c**, the title compound was obtained as a yellow-green solid product (21.0% yield).^{1}H NMR (400 MHz, Methanol-d_4) δ 8.78 (dd, J = 3.9, 2.2 Hz, 1H), 8.19 – 8.10 (m, 1H), 7.81 (dddd, J = 8.3, 6.9, 3.3, 1.3 Hz, 1H), 7.78 – 7.72 (m, 1H), 7.64 (dq, J = 9.6, 2.8 Hz, 1H), 7.54 (ddt, J = 8.2, 6.9, 2.8 Hz, 1H), 7.03 (dd, J = 8.6, 3.4 Hz, 1H), 3.80 (t, J = 7.0 Hz, 2H), 2.83 – 2.51 (m, 18H), 1.85 (dp, J = 21.1, 7.8, 7.2 Hz, 2H), 1.67 (dq, J = 16.2, 7.8 Hz, 2H). ^{13}C NMR (101 MHz, CD_3OD_SPE) δ 166.86, 159.35, 158.58, 145.91, 134.87, 133.79, 133.26, 126.17, 125.51, 122.20, 119.84, 119.33, 118.86, 113.73, 100.19, 72.47, 64.24, 54.90, 50.69, 44.96, 44.41, 26.38, 24.25. HRMS(ESI) m/z: ([M+H]$^{+}$) calcd. For $C_{27}H_{37}N_8O^{+}$：489.3085，Found: 489.3083. HPLC:>99%

2-(4-((4-(1,4,7,10-tetraazacyclododecan-1-yl)butyl)amino)quinazolin-2-yl)-4-methylphenol (4g)

Following General Procedure 4 using reactant **3f**, the title compound was obtained as a yellow solid product (19.0% yield). ^{1}H NMR (400 MHz, Methanol-d_4) δ 8.29 (d, J = 2.3 Hz, 1H), 8.15 (dd, J = 8.2, 1.3 Hz, 1H), 7.77 (ddd, J = 8.2, 6.8, 1.3 Hz, 1H), 7.72 (dd, J = 8.5, 1.4 Hz, 1H), 7.48 (ddd, J = 8.3, 6.8, 1.4 Hz, 1H), 7.17 (dd, J = 8.3, 2.4 Hz, 1H), 6.83 (d, J = 8.2 Hz, 1H), 3.80 (t, J = 6.7 Hz, 2H), 2.96 – 2.74 (m, 18H), 2.35 (s, 3H), 1.91 – 1.79 (m, 2H), 1.73 (td, J = 8.4, 4.3 Hz, 2H). ^{13}C NMR (101 MHz, CD_3OD_SPE) δ 161.30, 159.26, 158.74, 147.48, 132.78, 132.71, 129.02, 126.95, 126.08, 125.30, 122.04, 119.19, 116.77, 113.60, 53.81, 51.01, 45.68, 44.65, 43.74, 40.92, 26.56, 24.87, 19.66. HRMS(ESI) m/z: ($[M+H]^+$) calcd. For $C_{27}H_{40}N_7O^+$：478.3289，Found: 478.3294. HPLC:95.12%

methyl 3-(4-((4-(1,4,7,10-tetraazacyclododecan-1-yl)butyl)amino)quinazolin-2-yl)-4-hydroxybenzoate (4h)

Following General Procedure 3 using reactant **3g**, the title compound was obtained as a green solid product (67.0% yield).^{1}H NMR (400 MHz, Methanol-d_4) δ 9.10 (dq, J = 7.7, 2.4 Hz, 1H), 8.07 – 7.97 (m, 1H), 7.91 (dq, J = 8.4, 2.3 Hz, 1H), 7.78 – 7.59 (m, 2H), 7.44 (dq, J = 7.4, 4.4, 2.5 Hz, 1H), 6.95 – 6.84 (m, 1H), 3.90 (s, 3H), 3.82 – 3.61 (m, 2H), 3.01 – 2.41 (m, 18H), 1.91 – 1.50 (m, 4H). ^{13}C NMR (101 MHz, CD_3OD_SPE) δ 168.94, 167.12, 166.00, 160.67, 159.35, 147.02, 146.50, 133.02, 131.64, 125.75, 122.12, 119.50, 118.92, 117.41, 113.67, 54.29, 51.00, 50.82, 46.14, 44.60, 44.38, 40.95, 26.56, 24.57. HRMS(ESI) m/z: ($[M+H]^+$) calcd. For $C_{28}H_{40}N_7O_3^+$：522.3188，Found: 522.3179. HPLC:95.74%

2-(4-((4-(1,4,7,10-tetraazacyclododecan-1-yl)butyl)amino)quinazolin-2-yl)-4-chlorophenol (4i)

Following General Procedure 4 using reactant **3d**, the title compound was obtained as a green solid product (28.0% yield).^{1}H NMR (400 MHz, Methanol-d_4) δ 8.41 (t, J = 2.1 Hz, 1H), 8.14 – 8.07 (m, 1H), 7.80 – 7.74 (m, 1H), 7.71 (dd, J = 8.4, 1.2 Hz, 1H), 7.49 (dddd, J = 8.3, 6.8, 3.4, 1.4 Hz, 1H), 7.29 (dd, J = 8.8, 2.8 Hz, 1H), 6.91 (d, J = 8.8 Hz, 1H), 3.79 – 3.70 (m, 2H), 3.02 – 2.48 (m, 18H), 1.82 (dp, J = 22.1, 7.1 Hz, 2H), 1.73 – 1.58 (m, 2H). ^{13}C NMR (101 MHz, CD_3OD_SPE) δ 165.33, 160.02, 159.74, 159.38, 147.03, 132.94, 131.45, 128.16, 125.74, 122.59, 122.09, 120.71, 118.61, 113.71, 55.37, 54.36, 50.86, 46.12, 44.57, 44.36, 40.84, 26.50, 24.58. HRMS(ESI) m/z: ($[M+H]^+$) calcd. For $C_{26}H_{37}ClN_7O^+$：498.2743，Found: 498.2739. HPLC:>99%

3-(4-((4-(1,4,7,10-tetraazacyclododecan-1-yl)butyl)amino)quinazolin-2-yl)-4-hydroxybenzonitrile Platinum complex (5a; 4f-Pt)

Following General Procedure 5 using reactant K_2PtCl_4, the title compound was obtained as a red solid product. (83.0% yield). HRMS(ESI) m/z: ($[M+H]^+$) calcd. For $C_{27}H_{35}N_8OPt^+$：682.2577，Found: 682.1438.

3-(4-((4-(1,4,7,10-tetraazacyclododecan-1-yl)butyl)amino)quinazolin-2-yl)-4-hydroxybenzonitrile Copper complex (5b; 4f-Cu)

Following General Procedure 5 using reactant $Cu(NO_3)_2$, the title compound was obtained as a blue solid product. (73.0% yield).

HRMS(ESI) m/z: ($[M+H]/2^+$) calcd. For $C_{27}H_{36}CuN_8O_2^+$：275.6149，Found: 275.6408.

3-(4-((4-(1,4,7,10-tetraazacyclododecan-1-yl)butyl)amino)quinazolin-2-yl)-4-hydroxybenzonitrile Zinc complex (5c; 4f-Zn)

Following General Procedure 5 using reactant $Zn(NO_3)_2 \cdot 6H_2O$, the title compound was obtained as a white solid product. (86.0% yield).

HRMS(ESI) m/z: ($[M+H]^+$) calcd. For $C_{27}H_{35}N_8OZn^+$：551.2220，Found: 551.2238.

4.2. EGFR kinase inhibition assay

All enzymatic reactions for tyrosine kinases were performed at room temperature (approximately 25 °C) for 30 min, following the LanthaScreen® assay protocol recommended by Invitrogen. The reaction mixture (20 μL) contained 50 mM HEPES (pH 7.5), 10 mM $MgCl_2$, 0.01% Tween-20, 0.01% BSA, 2 mM DTT, 10 μM ATP, and the respective recombinant kinase. Fluorescein-Poly GT was used as the substrate at a final concentration of 0.2 mg/mL. Test compounds were diluted in 100% DMSO, then serially diluted to generate ten concentrations. 200 nL of each dilution was transferred into 384-well assay plates using an Echo liquid handler. The final DMSO concentration in each well was maintained at 1%. Kinase reactions were initiated by the addition of the substrate solution and terminated after 30 min by the addition of a detection solution containing Tb-PY20 antibody, followed by incubation for 60 min at room temperature. TR-FRET signals were measured using an EnVision plate reader with excitation at 340 nm and dual emission at 495 nm and 520 nm. The ratio of 520 nm/495 nm fluorescence intensities was used to calculate percent inhibition according to the equation: %Inhibition = (Max − Sample)/(Max − Min) × 100, where “Max” is the DMSO control and “Min” is the no-enzyme control. IC_{50} values were determined by nonlinear regression of normalized dose–response data using XLFit (v5.4.0.8) in Microsoft Excel.

4.3. CCK-8 cell viability assay

PC-9, NCI-H1975, H1975/OR, and BEAS-2B cells were seeded into 96-well plates at 8,000 cells/well in 100 μL of complete culture medium and incubated overnight. The old medium was then aspirated, and 100 μL of fresh medium containing various concentrations of 4f was added. Each concentration was evaluated in two independent experiments. Vehicle-treated wells (containing an equivalent volume of DMSO) and blank wells (containing medium only, without cells) were included as controls. After 24 h of incubation, 10 μL of CCK-8 reagent was added to each well, and the plates were incubated for an additional 1–2 h at 37 °C in the dark. Absorbance at 450 nm was then recorded to calculate cell viability.

4.4. Plasmid DNA electrophoresis

The DNA cleavage activity of the compounds was evaluated by 1% agarose gel electrophoresis (90 V, 60 min) in 1 × TAE buffer at room temperature. Typically, 5 μL of the pUC18 DNA reaction samples mixed with the corresponding loading buffer were loaded on the gel. After 15 min of staining in SYBR Gold, the gels were imaged with a gel imaging system (Tanon-1600, China).

4.5. Alkaline comet assay and image analysis

NCI-H1975 cells were seeded in six-well plates and cultured for 24 h. Cells were then treated for 24 h with 4f (40 μM), 4f-Pt (154 μM), or 0.1% DMSO as the vehicle control. Harvested cells were resuspended in PBS and embedded in low-melting-point agarose on slides precoated with normal-melting-point agarose. Slides were lysed at 4 °C for 2 h and washed with PBS. DNA was unwound in alkaline electrophoresis buffer for 40 min, followed by electrophoresis at 30 V for 30 min in an ice bath. Slides were neutralized, stained with propidium iodide for 15 min in the dark, and imaged on a Leica Stellaris 5 confocal microscope.

Comet images were analyzed with the OpenComet v1.3.1 plugin for ImageJ. Background correction and automatic head detection were used for object identification. Objects classified by OpenComet as normal comets were included. Overlapping, edge-truncated, morphologically abnormal, and outlier objects were excluded. Tail DNA and Olive tail moment were recorded for each included comet. Four 10× fields were analyzed per condition, and field means are reported as mean ± SD. Images acquired at 10× and 20× were analyzed separately because moment-based measurements depend on pixel scale. All four fields came from one experimental batch; the data are therefore presented descriptively without inferential testing.

4.6. Computational analysis

The crystal structure of EGFR L858R/T790M/C797S (PDB: 6LUD) and a double-stranded DNA structure (PDB: 1BNA) were used for docking analyses. Compounds 4a and 4f were examined in the mutant EGFR pocket, whereas compounds 4f and 6b were examined with DNA. Binding poses were inspected for the ligand–protein and ligand–DNA contacts discussed in Sections 2.3 and 2.7. Electrostatic-potential mapping was used to visualize the charge distribution of 4f.

4.7. Annexin V-PE/7-AAD apoptosis assay

NCI-H1975 cells were seeded in six-well plates and cultured for 24 h. Cells were then treated for 24 h with 4f at 12.5, 25, or 50 μM, or with 0.1% DMSO as the vehicle control. Cells were harvested, washed twice with cold PBS, and resuspended in 1× Binding Buffer (BD #559763) at approximately 1×10^6 cells/mL. A 100 μL aliquot was transferred to a 5 mL polystyrene tube, mixed with 5 μL Annexin V-PE and 5 μL 7-AAD, and incubated for 15 min at room temperature in the dark. After addition of 400 μL Binding Buffer, samples were analyzed by flow cytometry within 1 h.

Supplementary material

Supplementary material (Online Resource 1) includes representative and quantitative comet-assay results (Fig. S1), EGFR kinase concentration–response curves (Figs. S2–S5), and the original NMR and HRMS spectra of the synthesized compounds.

Abbreviations

7-AAD, 7-aminoactinomycin D; CCK-8, Cell Counting Kit-8; Cu, copper; Del19, exon 19 deletion; DMSO, dimethyl sulfoxide; DNA, deoxyribonucleic acid; EGFR, epidermal growth factor receptor; ESP, electrostatic potential; H1975/OR, osimertinib-resistant NCI-H1975 cells; HRMS, high-resolution mass spectrometry; IC_{50}, half-maximal inhibitory concentration; NMR, nuclear magnetic resonance; NSCLC, non-small cell lung cancer; PDB, Protein Data Bank; PE, phycoerythrin; PI, propidium iodide; Pt, platinum; ROS, reactive oxygen species; SAR, structure-activity relationship; SD, standard deviation; TKI, tyrosine kinase inhibitor; WT, wild type; Zn, zinc.

Statements and Declarations

Funding

This work was supported by the Fundamental Research Funds for the Central Universities (PT2026-15), the Joint Project of BRCBC (Biomedical Translational Engineering Research Center of BUCT-CJFH) (XK2020-06), the Collaborative Innovation Research Fund of the BUCT-CZU Collaborative Innovation Center (BUCT-CZU-010), the Open Research Fund of the State Key Laboratory of Simcere (SKLSIM-20251431), and the National Natural Science Foundation of China (82474414 and 22177011). The funders had no role in study design; data collection, analysis, or interpretation; manuscript preparation; or the decision to submit the work for publication.

Competing interests

The authors declare that they have no known competing financial interests or personal relationships that could have appeared to influence the work reported in this paper.

Author contributions

Hao Chang: Conceptualization, methodology, investigation, data curation, visualization, and writing – original draft. Changyang Lei, Kai Liu, Cenjun Li, Fangke Zhi, and Wei Liu: Investigation and methodology. Cheng Zhang: Methodology, resources, and validation. Renzhong Qiao and Chao Li: Conceptualization, supervision, project administration, funding acquisition, and writing – review and editing. All authors reviewed and approved the final manuscript.

Data availability

The data supporting the findings of this study are available within the article and its supplementary material. Additional raw data are available from the corresponding author upon reasonable request.

Ethics declaration

This study did not involve human participants or animal experiments.

Safety statement

No unexpected or unusually high safety hazards were encountered.

References

1. Gridelli C, Rossi A, Carbone DP, Guarize J, Karachaliou N, Mok T, et al. Non-small-cell lung cancer. Nat Rev Dis Primers. 2015;1:15009. https://doi.org/10.1038/nrdp.2015.9

2. Paez JG, Jänne PA, Lee JC, Tracy S, Greulich H, Gabriel S, et al. EGFR mutations in lung cancer: correlation with clinical response to gefitinib therapy. Science. 2004;304:1497–1500. https://doi.org/10.1126/science.1099314

3. Wu YL, Cheng Y, Zhou X, Lee KH, Nakagawa K, Niho S, et al. Dacomitinib versus gefitinib as first-line treatment for patients with EGFR-mutation-positive non-small-cell lung cancer (ARCHER 1050): a randomised, open-label, phase 3 trial. Lancet Oncol. 2017;18:1454–1466. https://doi.org/10.1016/S1470-2045(17)30608-3

4. Nelson V, Ziehr J, Agulnik M, Johnson M. Afatinib: emerging next-generation tyrosine kinase inhibitor for NSCLC. Onco Targets Ther. 2013;6:135–143. https://doi.org/10.2147/OTT.S23165

5. Kobayashi S, Boggon TJ, Dayaram T, Jänne PA, Kocher O, Meyerson M, et al. EGFR mutation and resistance of non-small-cell lung cancer to gefitinib. N Engl J Med. 2005;352:786–792. https://doi.org/10.1056/NEJMoa044238

6. Zhou W, Ercan D, Chen L, Yun CH, Li D, Capelletti M, et al. Novel mutant-selective EGFR kinase inhibitors against EGFR T790M. Nature. 2009;462:1070–1074. https://doi.org/10.1038/nature08622

7. Soria JC, Ohe Y, Vansteenkiste J, Reungwetwattana T, Chewaskulyong B, Lee KH, et al. Osimertinib in Untreated EGFR-Mutated Advanced Non-Small-Cell Lung Cancer. N Engl J Med. 2018;378:113–125. https://doi.org/10.1056/NEJMoa1713137

8. Zhao S, Xu Z. Development of indole hybrids for potential lung cancer treatment-part I: nitrogen-containing six-membered aromatic heterocycles. Future Med Chem. 2025;17:839–855. https://doi.org/10.1080/17568919.2025.2485675

9. Chen L, Fu W, Zheng L, Liu Z, Liang G. Recent progress of small-molecule epidermal growth factor receptor (EGFR) inhibitors against C797S resistance in non-small-cell lung cancer: miniperspective. J Med Chem. 2018;61:4290–4300. https://doi.org/10.1021/acs.jmedchem.7b01310

10. Du X, Yang B, An Q, Assaraf YG, Cao X, Xia J. Acquired resistance to third-generation EGFR-TKIs and emerging next-generation EGFR inhibitors. Innovation (Camb). 2021;2:100103. https://doi.org/10.1016/j.xinn.2021.100103

11. Wang S, Song Y, Liu D. EAI045: The fourth-generation EGFR inhibitor overcoming T790M and C797S resistance. Cancer Lett. 2017;385:51–54. https://doi.org/10.1016/j.canlet.2016.11.008

12. Uchibori K, Inase N, Araki M, Kamada M, Sato S, Okuno Y, et al. Brigatinib combined with anti-EGFR antibody overcomes osimertinib resistance in EGFR-mutated non-small-cell lung cancer. Nat Commun. 2017;8:14768. https://doi.org/10.1038/ncomms14768

13. Ju Y, Wu J, Yuan X, Zhao L, Zhang G, Li C, et al. Design and evaluation of potent EGFR inhibitors through the incorporation of macrocyclic polyamine moieties into the 4-anilinoquinazoline scaffold. J Med Chem. 2018;61:11372–11383. https://doi.org/10.1021/acs.jmedchem.8b01612

14. Chang H, Zhang C, Liang Z, Liu F, Zhang Y, Tian J, et al. Structure-guided discovery of a potent 2-aryl-4-aminoquinazoline-based inhibitor overcoming osimertinib resistance driven by EGFR C797S mutation in NSCLC. Eur J Med Chem. 2026;311:118818. https://doi.org/10.1016/j.ejmech.2026.118818

15. Chang H, Qiao R, Li C. Recent advances in functionalized macrocyclic polyamines for medicine applications. Chin Chem Lett. 2025;36:110675. https://doi.org/10.1016/j.cclet.2024.110675

Supplementary Files

This is a list of supplementary files associated with this preprint. Click to download.

- SupportingInformationMCR.pdf
- GraphicalAbstract.tif